Generative adversarial networks for reconstructing natural images from brain activity

K. Seeliger,* U. Güçlü, L. Ambrogioni, Y. Güçlütürk, M. A. J. van Gerven

Radboud University
Donders Institute for Brain, Cognition and Behaviour
Montessorilaan 3, 6525 HR Nijmegen, The Netherlands

December 8, 2017

Abstract

We explore a straightforward method for reconstructing visual stimuli from brain activity. Using large databases of natural images we trained a deep convolutional generative adversarial network capable of generating gray scale photos, similar to stimuli presented during two functional magnetic resonance imaging experiments. Using a linear model we learned to predict the generative model's latent random vector $\mathbf{z}$ from measured brain activity. The objective was to create an image similar to the presented stimulus image through the previously trained generator. Using this approach we were able to reconstruct natural images, but not to an equal extent for all images with the same model. A behavioral test showed that subjects were capable of identifying a reconstruction of the original stimulus in 67.6% and 64.4% of the cases in a pairwise test for the two natural image datasets respectively. Our approach does not require end-to-end training of a large generative model on limited neuroimaging data. As the particular GAN model can be replaced with a more powerful variant, the current advances in generative modeling promise further improvements in reconstruction performance.

1   Introduction

Since the advent of functional magnetic resonance imaging (fMRI), numerous new research directions that leverage its exceptional spatial resolution, leading to classifiable brain activity patterns, have been explored (Haynes, 2015). New approaches to decoding specific brain states have demonstrated the benefits of pattern-based fMRI analysis. Pattern-based decoding from the visual system has shown that it is possible to decode edge orientation (Kamitani and Tong, 2005), perceived categories of both static and dynamic stimuli (Haxby, 2001; Huth et al., 2016), up to identifying a specific stimulus image (Kay et al., 2008) and generically identifying new categories from image descriptors predicted from brain activity (Horikawa and Kamitani, 2017).

Here we focus on an advanced problem in brain decoding, which is actually reconstructing a perceived (natural) visual stimulus. The reconstruction problem is demanding since the set of possible stimuli is effectively infinite. This problem has been explored at different spatial scales (e.g. invasively on the cellular level (Chang and Tsao, 2017)) and in different regions of the visual system (e.g. in the LGN (Stanley et al., 1999), in the retina (Parthasarathy et al., 2017)). Here we focus on image reconstruction from brain activity measured with fMRI. This area was pioneered by Thirion et al. (2006), who reconstructed dot patterns with rotating Gabors from perception and imagery. Miyawaki et al. (2008) used binary 10×10 images as stimuli and demonstrated

---

*Corresponding author: ✉ kseeliger@posteo.jp

the possibility of decoding pixels independently from each other, reconstructing arbitrary new images with this basis set. Naselaris et al. (2009) introduced a combination of encoding brain activity with structural and semantic features, as well as a Bayesian framework to identify the most likely stimulus image from a very large image database given the brain activity. Combining the most likely stimuli from a database leads to effective reconstructions, with (Nishimoto et al., 2011) being the most impressive example to date. Bayesian approaches were further developed. Examples are enhancing decoding using feature sets learned with independent component analysis (Güçlü and van Gerven, 2013) and accurate reconstruction of handwritten characters using stimulus domain priors and a linear model for predicting brain activity (Schoenmakers et al., 2013, 2015). The most recent entries in the reconstruction domain make use of promising new developments in generative image models. Du et al. (2017) used Bayesian inference to derive missing latent variables, and effectively reconstruct handwritten digits and 10×10 binary images. Finally, adversarial training has been used for reconstructing face photos from fMRI with high detail by learning to encode to and decode from a learned latent space for faces (Güçlütürk et al., 2017).

In this work we expand on the generative model idea, but explore the capabilities of a method that applies a natural image generative model as a black box which is trained without using (usually limited) neuroimaging data. We pretrain a deep convolutional generative adversarial network (DCGAN) (Radford et al., 2015), capable of producing arbitrary images from the stimulus domain (handwritten characters or natural gray scale images). Keeping this GAN fixed we learn to predict the latent space of the generator $\mathbf{z}$ based on the fMRI BOLD signal in response to a presented stimulus. The objective is achieving high similarity between the generated and the original image in the image domain. The image domain losses that are used to train the predictive model are derived with a complex loss function. We show that this approach is capable of generating reasonable reconstructions from fMRI data for the given stimulus domains.

2 Methods

2.1 Functional MRI data sets

We made use of three publicly available fMRI data sets originally acquired for experiments related to identifying stimulus images and categories or reconstruction of perception. In the following we briefly list their properties. Extensive descriptions of recording details and methods can be found in the original publications.

2.1.1 Handwritten characters

We used this dataset (referred to as `BRAINS` dataset) to test our method in a simpler, restricted domain. Three subjects were presented with gray scale images of 360 examples of six handwritten characters (B, R, A, I, N and S; as published with Van der Maaten (2009); Schomaker and Vuurpijl (2000)) with fixation in a 3T fMRI experiment (TR=1.74 s, voxel size=2 mm³). The images were shown for 1 s at $9 \times 9°$ of visual angle, flashed at approximately 3 Hz. The characters were repeated twice, and responses were averaged. The original studies reconstructed handwritten characters using a linear decoding approach (Schoenmakers et al., 2013) and Gaussian mixture models (Schoenmakers et al., 2015). We made use of the preprocessed data from V1 and V2 available in the BRAINS dataset and used the original train / test set split (290 and 70 characters respectively). The dataset can be downloaded from `www.artcogsys.com`.

2.1.2 Masked natural images

Three subjects saw natural gray scale images with a circular mask, taken from different sources (the commercial Corel Stock Photo Libraries from Corel Corporation, and the Berkeley Segmentation Dataset) at $20 \times 20°$ of the visual field with fixation. The dataset and experiments were

described in (Kay et al., 2008) and (Naselaris et al., 2009). The training set consisted of 1750 images, presented twice and averaged. The test set consisted of 120 images, presented 13 times. Images were presented for 1 s and flashed at approximately 3 Hz. Data was acquired in a 4T scanner (TR=1 s, voxel size=2 $\times$ 2 $\times$ 2.5 mm^3). The dataset is available on www.crcns.org under the identifier vim-1[1], which is also how we refer to it in this manuscript. We obtained a version of the dataset with updated preprocessing for all three subjects from the author via personal communication. In our study we used the first 50 images from the original validation dataset as a test set, and the remainder of the data for training. The advantage of the dataset for this study is the amount of data and the variety of high-quality photo stimuli.

2.1.3 Natural object photos

This dataset was originally recorded for (Horikawa and Kamitani, 2017), and is referred to as Generic Object Decoding dataset. Five subjects were presented with square colour images from 150 categories from the ImageNet database (Deng et al., 2009). We converted the stimulus images to gray scale and applied a similar mild contrast enhancement as in (Kay et al., 2008) instead of using the full color stimuli for reconstruction[2]. We also used the original train / test set split. The training set consisted of 8 images from each category and was presented once, totaling 1200 presentations. The test set recording consisted of presenting single images of 50 categories (*not* contained in the training set) 35 times each, and averaging this activity. The data can be obtained from www.brainliner.jp[3]. Next to having recordings of five subjects one advantage of this dataset is the long stimulation time of 9 s (at 2 Hz flashing) per image, resulting in a high signal-to-noise ratio (SNR). All images were presented at 12 $\times$ 12° of visual angle, with fixation, in a 3T scanner (TR=3 s, voxel size= 3 mm^3).

The data of the individual subjects of all datasets were mapped to a common representational space based on hyperalignment (Haxby et al., 2011) using PyMVPA[4] (Hanke et al., 2009). Hyperaligned data was averaged across subjects such as to obtain data for a single hyperaligned subject with improved SNR[5]. After hyperalignment, the dimensionality of the feature (voxel activity) space was reduced by applying principal component analysis (PCA, including demeaning) so that 99% (BRAINS, Generic Object Decoding) or 90% (vim-1, due to its much larger voxel dimension) were preserved. Hyperalignment, PCA and statistical parameters (e.g. mean values) were computed on the training sets and applied on the training and the separate test set. For these additional preprocessing steps we used the single trial data for vim-1 and Generic Object Decoding, as the different averaging strategies changed SNR between train and test. For BRAINS we used the provided data averages over two trials as there was no such difference between the train and test recordings.

2.2 Generative Adversarial Networks

Generative Adversarial Networks (GANs) learn to synthesize elements of a target distribution p_{data} (e.g. images of natural scenes) by letting two neural networks compete. Their results tend to have photo-realistic qualities. The Generator network (G) takes an n-dimensional random sample from a predefined distribution – conventionally called latent space $\mathbf{z}$ – and attempts to create an example $G(\mathbf{z})$ from the target distribution, with $\mathbf{z}$ as initial values. In the case of images and deep convolutional GANs (DCGANs), introduced in (Radford et al., 2015), this is realized

---

[1] https://crcns.org/data-sets/vc/vim-1 (last access May 2017)

[2] We focus on reconstructing gray scale images as our natural images DCGAN learned to generate more structural detail when the color dimension was omitted. However with a more powerful GAN variant the method could also be applied for reconstructing color stimuli.

[3] http://brainliner.jp/data/brainliner/Generic_Object_Decoding (last access August 2017)

[4] www.pymvpa.com, v2.6.3

[5] Our method was initially developed on the individual subject basis. This only seemed to lead to more variability in the reconstruction quality between subjects, and we decided to finalize the study on hyperaligned data instead as this made collecting behavioral data and developing the loss function more efficient.
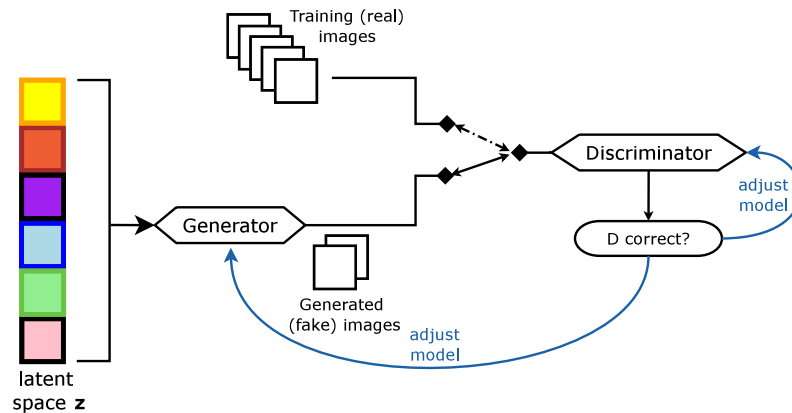
Figure 1: Generative adversarial networks. A generator network (G) learns to model a given distribution p_{data} via feedback from a discriminator network (D). D learns to discriminate between images coming from the real distribution and images from the generator.

across a series of deconvolutional layers. The Discriminator network (D) takes a generated or real example as input and has to make the binary decision whether the input is real or generated, which would result in the output 1 or 0, respectively. In the discriminator, DCGANs use a series of convolutional layers with a binary output. See Figure 1 for an illustration. This competition process is expressed as a zero-sum game in the following loss term:

$$\min_D \max_G \quad \log(D(\mathbf{x})) + \log(1 - D(G(\mathbf{z}))) \tag{1}$$

where $\mathbf{x}$ is a real image and $G(\mathbf{z})$ a generated image. During training, various – but certainly not all – GAN variants learn to impose structure on the latent space. Learning this structure and the learning procedure itself is a form of unsupervised learning. The algorithm we use was introduced and popularized for image synthesis by (Goodfellow et al., 2014). Creswell et al. (2017) is a recommended comprehensive review and discussion of various recent GAN approaches.

For this work we used a DCGAN architecture that implements architectural improvements suggested in (Radford et al., 2015) and (Salimans et al., 2016). We based the model on a publicly available framework and implementation (`musyoku`, 2017). The *generator network* consists of one linear and four deconvolutional layers, each followed by batch normalization and ReLU activation functions. The linear layer takes $\mathbf{z}$ and maps it to the first deconvolutional layer that expects 512 feature channels via $512 \times 64 \times 64$ output values in order to match the target image dimension. The generator then maps to 256, 128, 64 and 1 feature channels across the deconvolutional layers. Kernel sizes are 4×4 and stride is 2 in every deconvolutional layer. The pixel output of the generator is scaled between $[-1, 1]$ by applying $\tanh$ to the output values as a final step. Numerical instabilities required additional clipping of the generated pixel values at $[-1, 1]$. A feature matching loss, using the first discriminator layer, was also added to the generator loss term. For the `vim-1` DCGAN we manually apply the circular mask used for creating the stimuli at the end of training in order to let the training process focus on the visible area. The *discriminator network* consists of 4 convolutional layers, followed by batch normalization and ELU activations (Clevert et al., 2015). Before the image enters the discriminator handicap Gaussian noise with a standard deviation of 0.15 is added to the input images. Except in the initial layer (which had 3x3 kernels) all layers use kernel sizes of 4x4 and a stride of 2. The layers map from 1 to 32, then 64, 128 up to 256 feature channels, and are followed by a linear layer mapping all final activations to a single value reflecting the discriminator decision.

The latent variable $\mathbf{z} \in [-1, 1]^{50}$ is randomly drawn from a uniform distribution and restricted to a unit hypersphere by normalizing it, in order to embed it in a continuous bounded space without borders. This step facilitates the prediction of $\mathbf{z}$ in an otherwise unbounded solution

to the regression problem. For optimizing the weights of the DCGAN we used the Adam optimizer (Kingma and Ba, 2014) with default parameters ($\alpha = 0.001$, $\beta_1 = 0.9$, $\beta_2 = 0.999$, $\epsilon = 10^{-8}$). The learning rate was 10^{-4} for all networks. We applied gradient clipping with a threshold of 10.

As DCGAN training data we used a downsampled 64×64 variant of ImageNet (made available with (Chrabaszcz et al., 2017)) together with the Microsoft COCO dataset[6]. The image size of MS COCO was decreased to 64×64 and center-cropped, and images for which this was not possible due to aspect ratio were removed from the training set. Before entering training all images were converted to gray scale and contrast-enhanced with `imadjust` (as in `MATLAB`), similar to the transformation used in (Kay et al., 2008). The image value range entering training was $[-1, 1]$. For the `vim-1` GAN, again the circular mask was applied. This resulted in approximately 1.500.000 gray scale natural images used for training in total. Note that DCGAN training would usually also work with a lower amount of training data.

The DCGAN on handwritten characters was trained on (in total) 15.000 examples of B, R, A, I, N and S characters from (Van der Maaten, 2009) and (Schomaker and Vuurpijl, 2000). As the experiment on the `BRAINS` dataset should focus on a restricted stimulus domain its DCGAN does not require more expressive power.
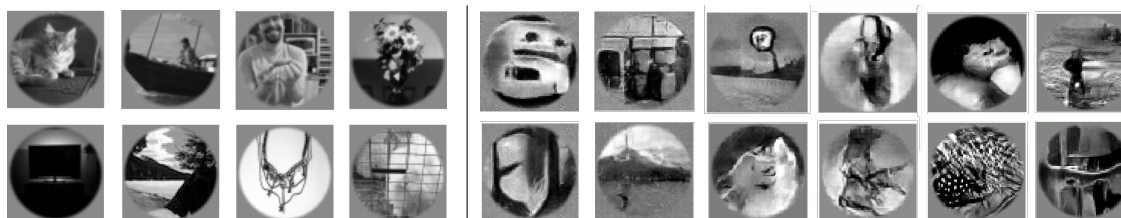

Figure 2: Training a DCGAN for naturalistic `vim1`-like gray scale images. Left: Examples from the gray scale natural image domain DCGAN training set (gray scale MS COCO or ImageNet; masked). Right: Examples of images randomly generated by a trained natural image DCGAN.

We trained the same DCGAN architecture separately for each dataset, for approximately 300 iterations through all training images. Figure 2 shows examples from the `vim-1` training set, and randomly generated examples from a DCGAN trained on this data. The network seems to have learned the contrast properties of the `vim-1` stimulus set, and seems to have acquired the ability to create complex image content. As we selected these random example images manually they reflect our preference for semantically meaningful content. Yet, as with most GAN architectures, much of what is created is rather abstract and can not be interpreted. The handwritten character GAN in contrast learned to create primarily meaningful new examples of the reduced handwritten character set. We noticed that it rarely generated B examples though. So the DCGAN architecture we are using likely suffers from a form of the so far unsolved problem of mode collapse.

We checked whether the expressive power of our DCGAN is sufficient for reconstructing stimuli from the experiments by overfitting the model predicting **z** from BOLD data on the training data. For this we used a multi-layer perceptron (MLP) instead of the linear regression approach outlined in the following section 2.3. In Figure 3 we show training set reconstructions on `vim-1` from such an overfitted model. These examples can also be seen as an upper limit of the accuracy that can be expected with the DCGAN architecture used here. It is obvious that especially broad high-contrast boundaries can be reconstructed, but the natural images DCGAN also seems to capture patterns, luminance, luminance gradients and some of the semantic content (e.g. landscapes) that are in the stimulus set. We thus can state that the natural image DCGAN reflects the reconstruction target sufficiently. We assume but can not verify that semantic content can be reproduced if structural properties of the image restrict the semantic space. For instance, landscape photos frequently feature a horizontal bar across the whole image.

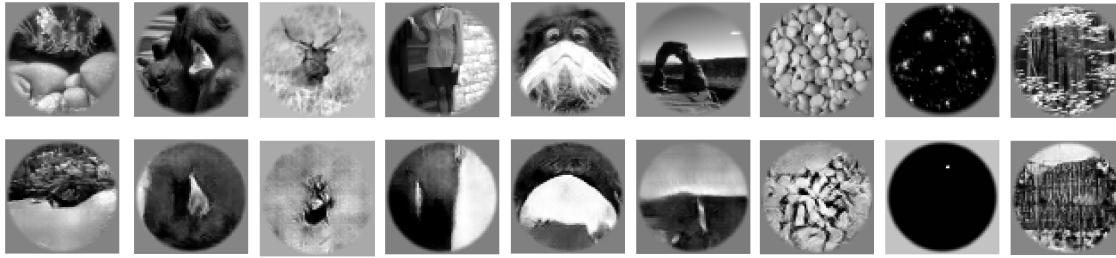[6]`www.mscoco.org`, described in (Lin et al., 2014) (last access March 2017)

Figure 3: The natural images GAN captures the `vim-1` training stimuli. We overfitted the model on random training set images to demonstrate that the latent space the GAN has learned is powerful enough to capture and regenerate the variety of the `vim-1` stimulus images satisfactorily. The top row shows the original stimulus image, the bottom row the overfitted reconstruction.

2.3   Latent space estimation from BOLD data

We fixed the trained DCGANs and attempted to predict the latent space $\mathbf{z}$ that reproduces the correct image directly with the BOLD data as the independent variable for every image. The loss for this model was gathered in image space with a complex multi-component loss function that compares the real and the reconstructed images with pixel and perceptual features learned by a convolutional neural network. The linear regression model was implemented as an approximating neural network with one weight layer. The procedure is illustrated in Figure 4. For weight optimization we used the Adam optimizer (Kingma and Ba, 2014), again with default parameters. We applied a mild L2-regularization on the weights ($\lambda_{L2} = 0.01$). The same normalization that we used as a boundary on $\mathbf{z}$ when training the GAN was applied to the predicted $\mathbf{z}$ after applying the linear regression weights.
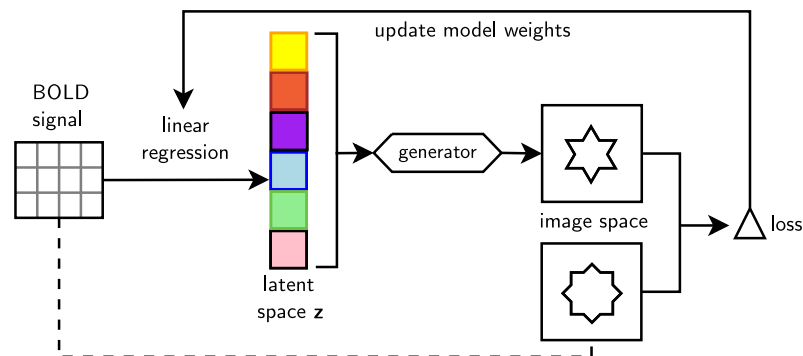

Figure 4: Predicting z from BOLD data with a complex loss function in image space between the reconstructed image and the image actually shown in the experiment. We make use of the DCGAN generator, which is pretrained for the necessary stimulus domain and not updated further during reconstruction model training.

For training the model, we passed the predicted latent vector $\mathbf{z}$ for every batch (of size 3) through the previously trained generator network G. The image produced by the generator $G(\mathbf{z})$ (reconstructed) was compared to the image $\mathbf{x}$ actually shown in the experiment with a complex image loss function that is a weighted sum of the following components (formulated as an average over mini batches):

Mean squared error on pixels   The $(64, 64)$ images were reduced in size by 10% to avoid some of the blurring effects of pixel-wise loss functions. Then mean squared error (MSE) was calculated

6

between them to obtain the pixel loss l_{px}:

$$l_{px} = \frac{1}{n} \sum_{k=1}^{n} ||\mathbf{x}^{(k)} - G\left(\mathbf{z}^{(k)}\right)||^2 \tag{2}$$

where k ranges over images in the image batch of length n [7].

Feature losses   Weights learned by convolutional neural networks on natural image data present a set of low- and intermediate level feature detectors useful for various applications. In methods such as autoencoders a feature-based loss seems to lead to higher perceptual similarity, whereas using pixel-wise loss functions such as MSE leads to blurry results (Johnson et al., 2016). We trained a variant of the AlexNet neural network to obtain suitable feature detectors (Krizhevsky et al., 2012).

For computing the loss between $G(\mathbf{z})$ and $\mathbf{x}$ on the basis of features from the trained AlexNet hierarchy we used two loss components. The first is *feature presence loss* $l_{f,b}$, which determines whether features are activated above a threshold at all. The feature activation matrices for one AlexNet layer L, denoted $\phi_L(\mathbf{x})$ and $\phi_L(G(\mathbf{z}))$ were transformed to binary representations $\phi_{L,b}(\mathbf{x})$ and $\phi_{L,b}(G(\mathbf{z}))$ by applying a threshold of 1.0. These binarized activation matrices were then flattened to their one-dimensional representation and compared via cross entropy loss[8]. A similar loss formulation is used in machine learning literature for multi-class classification. This yields

$$l_{f,b} = -\frac{1}{n} \sum_{k=1}^{n} \sum_{L} \phi_{L,b}\left(\mathbf{x}^{(k)}\right) \log\left(\phi_{L,b}\left(G\left(\mathbf{z}^{(k)}\right)\right)\right) - \left(1 - \phi_{L,b}\left(\mathbf{x}^{(k)}\right)\right) \log(1 - \phi_{L,b}\left(G\left(\mathbf{z}^{(k)}\right)\right)). \tag{3}$$

Feature activations were gathered before any nonlinearities or local response optimization. The second element of the feature losses and third component of the complete reconstruction loss function is *feature magnitude loss* $l_{f,m}$, which equates mean squared error computed between $\phi_L(\mathbf{x})$ and $\phi_L(G(\mathbf{z}))$ on feature map elements that met the binarization threshold in $\phi_{L,b}(\mathbf{x})$:

$$l_{f,m} = \frac{1}{n} \sum_{k=1}^{n} \sum_{L} ||\bar{\phi}_L\left(\mathbf{x}^{(k)}\right) - \bar{\phi}_L\left(G(\mathbf{z}^{(k)})\right)||^2 \tag{4}$$

where $\bar{\phi}_L(\mathbf{u}) = \phi_L(\mathbf{u}) \odot \phi_{L,b}(\mathbf{u})$; $\odot$ denoting element-wise multiplication.

We used layers `conv1` and `conv2` for feature matching as these represent universal low-level features and simple patterns in the AlexNet architecture. The highest layers of AlexNet may otherwise represent sparse semantic properties, however higher convolutional layers did not seem to improve results. Furthermore matching the final layers may also drive the reconstruction towards the limited set of categories learned by AlexNet.

From `conv1` we also collected $l_{f,b}$ and $l_{f,m}$ on negative feature activations, using the threshold 1.0 on their absolute representation, as they are collected via meaningful convolutions in pixel space. Negative feature activations for higher layers are likely meaningless as they are not used during training.

The complete loss function is then given by

$$loss = \lambda_{px} l_{px} + \lambda_{f,p} l_{f,p} + \lambda_{f,m} l_{f,m} \tag{5}$$

where we chose $\lambda_{px} = 10.0$, $\lambda_{f,p} = 50.0$ and $\lambda_{f,m} = 1.0$ for all three datasets. The values were determined via optimizing on the training set of `BRAINS`. Optimization specifically for each data set may improve the results further, however a cross-validated hyperparameter search would require more data than we had available.

---

[7]A proposed alternative for plain MSE loss would be using SSIM losses (Ridgeway et al., 2015). However, we instead decided to enhance this loss with a series of feature (perceptual) losses.

[8]It is not advisable to use MSE between feature activations as the feature activation matrices across a convolutional neural network hierarchy for any given image tend to be sparse. Due to this when using MSE our model frequently fell into a local minimum of feature activations with the value 0, which equates blurry images without prominent edges or features. Cross-entropy loss imposes a higher penalty on missing or obsolete features.

Feature matching networks   Feature matching requires a universal set of image descriptors that frequently occur in our chosen natural images p_{data}. To obtain these descriptors we trained a variant of AlexNet (Krizhevsky et al., 2012), with one input channel and 5×5 kernels in the first (`conv1`) layer on the 64×64 grayscale ImageNet data described before. The model was trained towards classifying the standard set of ImageNet categories. We used this network for `vim-1` and `Generic Object Decoding`, ignoring potential redundancy of features extracted from the mask in the former. For the `BRAINS` data set we again trained an AlexNet architecture. In this case we trained on all 40.000 examples of 36 handwritten digit and character classes from (Van der Maaten, 2009) and (Schomaker and Vuurpijl, 2000) in order to obtain a universal set of image descriptors for the handwriting domain.

Reconstruction variability   One inherent disadvantage of training models with random components, such as randomly initialized weights or stochastic gradient descent (e.g. neural networks) is the variability of the results, due to different local minima the model will converge to. Furthermore, in the case of GANs small shifts in the predicted latent space can result in well-perceivable changes in the generated image. We observed this behaviour, which resulted in the model finding different ways to reconstruct certain images, reconstructing different features of images, or not finding a recognizable reconstruction at all for an image that could be reconstructed in previous models. This variability is demonstrated in Figure 8. We attempted to counteract these effects when obtaining final reconstructions with a simple ensemble model: We averaged the predicted **z** over 15 independent training runs, normalizing **z** to the unit hypersphere again after this.

The feature matching networks, the natural images GAN and the predictive model for **z** have all been implemented in the `Chainer` framework for neural networks (Tokui et al., 2015)[9].

3   Results

Using the outlined methods and parameters we obtained a set of validation set reconstructions for each data set, out of which we show examples of reconstructed images and failure cases in the following. We proceeded with a quantitative behavioural evaluation of overall recognizability on these sets.

3.1   Reconstruction examples

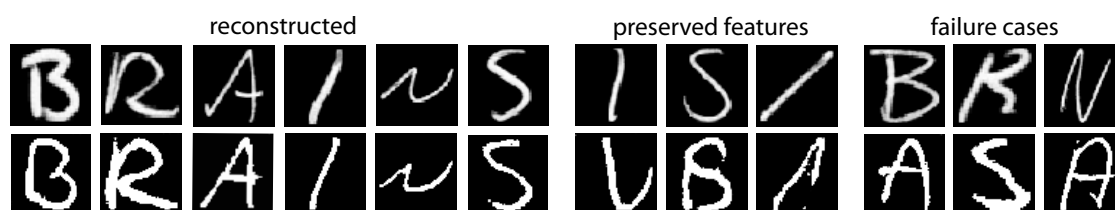### 3.1.1   Sample reconstructions on **BRAINS**

Figure 5: Reconstruction examples for handwritten characters. Top row: Presented stimuli. Bottom row: Reconstructions from BOLD activity.

Figure 5 demonstrates that the method can lead to accurate reconstructions when the DCGAN is restricted to few handwritten characters classes. Despite a small training set of 290 BOLD images of V1 and V2, the correct handwritten character is reconstructed in 57% of the cases (determined via human rating; chance level: 17%). Successful reconstructions demonstrate that

---

[9]www.chainer.org; Chainer v1.24

the model is also capable of reconstructing structural features such as position and curvature of lines. When character classes could not be reconstructed frequently such structural similarities remained. As mentioned before, the underlying handwritten character DCGAN had difficulties generating examples of B, and the reconstruction model also failed to reconstruct a B stimulus in 9 out of 12 cases.

3.1.2 Sample reconstructions on `vim-1`

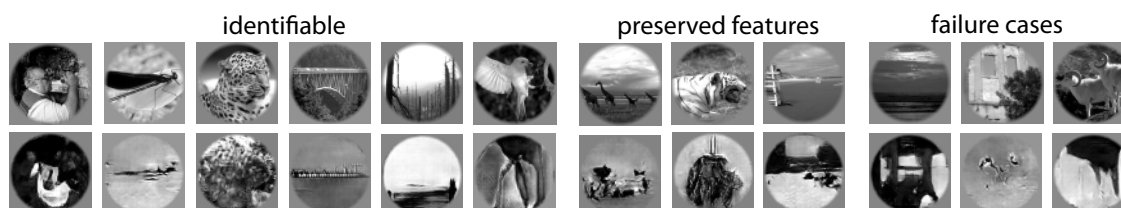identifiable   preserved features   failure cases

Figure 6: Reconstruction of natural grayscale images (`vim-1`). Top row: Presented images. Bottom row: Reconstructions from BOLD activity. Images in the *identifiable* category are reconstruction examples correctly assigned in no less than 4 of the 5 behavioural comparisons.

Figure 6 contains reconstruction examples for natural grayscale stimuli from the `vim-1` dataset. At 1820 training examples it was the largest training data set we used. In reconstructions that were sufficiently accurate to be identifiable in the behavioural tests, contrast differences appear to be the most likely image feature preserved. Salient pattern information also remained intact. In some reconstructions luminance information is lost, while structural features remain. A horizontal contour line across the image appears to lead the model into generating a landscape image, however not in every case (e.g. see the second and fourth image of the identifiable category).

3.1.3 Sample reconstructions on `Generic Object Decoding`

identifiable   preserved features   failure cases

Figure 7: Reconstruction of natural grayscale images (`Generic Object Decoding`). Top row: Presented images. Bottom row: Reconstructions from BOLD activity. Images in the *identifiable* category are reconstruction examples correctly assigned in no less than 4 of the 5 behavioural comparisons.

The `Generic Object Decoding` dataset has just 1200 training examples, but high SNR due to long stimulation time. The stimuli are not masked, so overall more content needs to be reconstructed per image. Reconstruction examples can be seen in Figure 7. Overall the reconstructions again preserve salient contrasts, but turned out more blurry than the `vim-1` reconstructions. There are also more failure cases[10] .

---

[10]The influence of omitting the colour information contained in the original stimuli is unclear. Random generations from a DCGAN trained with RGB information missed the structural detail obtained in the grayscale variant (data not shown). When using this RGB DCGAN for reconstructing it was often possible to reconstruct the correct hue for an image and its components. In terms of structure in most cases it was only capable of reconstructing salient blobs however.

3.1.4   Reconstruction variability

Figure 8: Reconstruction variability. Reconstructions vary when using different feature weights (λ), and to a lesser extent when running the model with the same settings multiple times. This is caused by the sensitivity of the **z** space and by different minima the model may find in the DCGAN.

When using different model parameters and loss weights, and to a lesser extent across different runs with the same parameters the model was often reconstructing the same images in different ways (for identifiable reconstructions). We described the potential cause of this problem further in Section 2.3 and demonstrate these effects in Figure 8.

3.2   Behavioural evaluation

A number of successful reconstructions of natural images have reversed luminance information or only slight or transformed structural similarity. Due to this, potential similarity measures such as the structural similarity index can not be applied as the comparison task is too complex in the natural images case. In order to obtain a quantitative measure of reconstruction similarity on each data set we instead made use of human perceptual systems.

We conducted a behavioural perceptual study on Amazon Mechanical Turk[11]. The advantages of this platform over common university subject pools for collecting human labeling and uncomplex behavioural scientific data have been discussed and demonstrated (Mason and Suri, 2012). Workers were presented with one original image from the validation sets and had to chose between the real and one randomly chosen different reconstruction taken from the same validation set. Each of these choices was one Human Intelligence Task (HIT) compensated with 0.01$. As a preventive measure against fake completions and bots, workers had to hold the Masters status and have an approval rate of 95% or higher on the platform to qualify for our tasks. We repeated the procedure five times for each of the validation set images in each data set, paired with a different randomly chosen reconstruction from the set in every HIT. Every HIT was presented once, i.e. we did not use the platform's internal repetition mechanism for verification. Across all three validation sets we presented 850 of these comparisons in total (250 for each natural image set), which were processed by 38 individual workers.

Figure 9 shows worker performance for the validation images of the three data sets. The number of *correct decisions* denotes the total number of correct decisions across all HITs (comparisons). As there were five such HITs per reconstruction it is slightly skewed both by failure and well-identifiable reconstructions, but is a better representation of potential undecidedness. The number of correct decisions *by image* on the other hand applies a majority vote over the 5 decisions per image, representing the number of validation set images that could be correctly identified.

All results were significantly different from random choices with $p \ll 0.01$ based on a binomial test (see (Salzberg, 1997)). Although the BRAINS dataset model reconstructed the correct character class in a mere 56% of the validation set images, structural resemblance between the original characters and their reconstructions were still strong enough for 75% and 74.3% correct
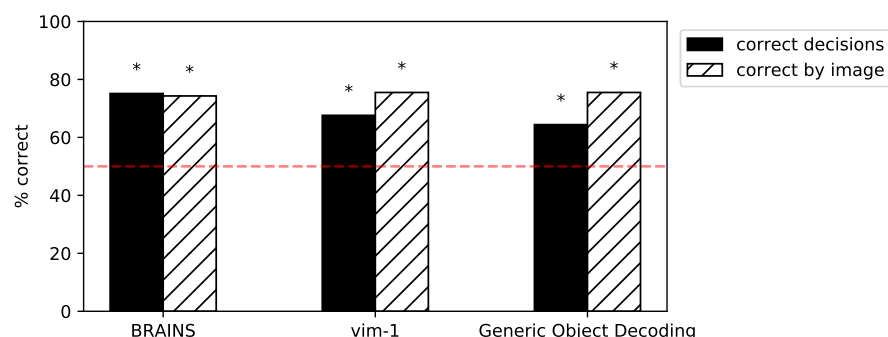
---

[11]www.mturk.com

Figure 9: Correctly identified reconstructions in pairwise behavioural test. Mechanical Turk workers were presented with an original image and had to chose its reconstruction out of two.

identifications based on overall and per-image decisions respectively. From the set of `vim-1` images workers correctly assigned 75.5% of the reconstructions, applying the majority vote per image. As for the overall number of correct decisions only 67.6% were correct, indicating that many reconstructions were still too crude to not be confused with a different random one. The `Generic Object Decoding` natural images stimulus set performed slightly worse at 64.4% correct overall, and 75.5% if grouped by image.

4 Discussion

We presented a new approach for reconstructing static visual stimuli with natural image characteristics from brain activity. We conducted a behavioural study indicating that the reconstructions this method achieves is sufficient for linking an original image to its reconstruction, even when reconstructing from the virtually infinite domain of natural images. Using a DCGAN generator as a pretrained natural image prior assures that the reconstruction results employ natural image statistics, preventing noisy images. An advantage of our method is that it does not require end-to-end training of a high number of complex neural network layers on usually limited neuroimaging data, using a pretrained DCGAN as a black box instead.

In the constrained domain of handwritten characters the correct character class could not be reconstructed in all cases, but the accuracy was still well above chance level. The method could furthermore reconstruct sufficient structural detail so that the right reconstruction could often still be identified in the behavioural test, even when the reconstructed character was incorrect. In this simpler, restricted domain the model showed good performance with a very limited amount of training data. However the DCGAN had difficulties generating one of the six characters. Nevertheless results indicate that the method can be applied for reconstructing stimuli from such a limited domain with high accuracy when making sure that all potential stimulus manifestations occur in the reconstruction model.

In Figure 3 we demonstrated on training set examples that the DCGAN captured much of the variety of the `vim-1` natural grayscale image set. While we can state that our results present a step forward over previous models, the reconstruction quality and generalization performance on the validation set certainly leave much to be desired. It is possible that generalization performance could increase by merely adding much more training data. Although both our natural image data sets contained less than 2000 training images (an insufficient amount for many machine learning methods), due to the difficulties of neuroimaging experiments `vim-1` and `Generic Object Decoding` are already considered large experimental data sets within the community. Yet for reconstruction studies such as ours, massive amounts of high-SNR visual system data from single subjects may be necessary. Another related antagonist of the generalization capabilities of our approach is the noisy nature of neuroimaging data which does not agree with the

sensitivity of the latent space. Subtle changes in $\mathbf{z}$ induced by noise in the brain data are capable of strongly changing the features of the reconstructed image. It is unclear whether this problem would remain in an experiment with much larger amounts of data with high quality.

Also, we achieved our results with a linear regression model. This linear relation promises interpretability of the relations between the latent space and brain representations, when the reconstruction model is powerful enough and sufficient care is applied. The latent space $\mathbf{z}$ of DCGANs has been shown to represent meaningful object properties, to the point of supporting vector arithmetic (Radford et al., 2015). The fact that we could achieve our results with a basic linear model also means that any more advanced regression model iteratively trained with a complex image loss function could further improve over our results.

Our loss function involves pixel luminance as well as edge and basic pattern information. We did not penalize the model on higher-order semantic information, e.g. by using the actual classifications or fully-connected layers from our feature matching network. The set of training classes of a convolutional neural network is always restricted to a specific subset. Our reconstructions would thus remain restricted to a predefined set of classes and could not be called arbitrary. Yet finding a valid method of adding a semantic penalty to the results could be another way of strongly improving over our results.

Our natural image GAN is set up to approximate the distribution of all natural grayscale images. This is still a constraint on the set of images that can be reconstructed. It will not be possible to reconstruct non-natural image types, such as handwritten characters or comic scenes; unless the generative model can been trained to generate images with non-natural statistics as well. A GAN trained on a specific image database such as ImageNet or MS COCO will reflect their potentially unbalanced selection of categories (e.g. dog breeds), which presents another bias. In the current development state GANs also easily fall into local minima where generated images show low variety. The generator can often fool the discriminator by learning a limited set of image types (modes of the image distribution) perfectly. This problem is known as *mode collapse*, and considered one of the most important issues to solve by the deep generative modeling community. One frequently explored remedy is providing binary categorical information along with $\mathbf{z}$ in a semi-supervised fashion. However, as mentioned before, such a discrete set of categories would present a severe limitation contradictory to our aim of reconstructing arbitrary images.

In conclusion we believe that our method and results present a promising foundation for future extensions. As generative modeling is one topic explored extensively in the machine learning community at the moment, drawbacks such as mode collapse may be solved in the near future. We believe reconstruction of arbitrary visual stimuli, imagination and even dreams is still a largely under-explored territory of neuroimaging research and will continue to strongly benefit from new advances in the machine learning community.

5   Funding

6   Acknowledgements

References

Chang, L. and Tsao, D. Y. (2017). The code for facial identity in the primate brain. *Cell*, 169(6):1013–1028.

Chrabaszcz, P., Loshchilov, I., and Hutter, F. (2017). A downsampled variant of ImageNet as an alternative to the CIFAR datasets. *arXiv preprint arXiv:1707.08819*.

Clevert, D.-A., Unterthiner, T., and Hochreiter, S. (2015). Fast and accurate deep network learning by exponential linear units (ELUs). *arXiv preprint arXiv:1511.07289*.

Creswell, A. P. N., White, T., Dumoulin, V., Arulkumaran, K., Sengupta, B., and Bharath, A. A. (2017). Generative adversarial networks: An overview. *arXiv preprint arXiv: 1710.07035*.

Deng, J., Dong, W., Socher, R., Li, L.-J., Li, K., and Fei-Fei, L. (2009). ImageNet: A large-scale hierarchical image database. In *IEEE Conference on Computer Vision and Pattern Recognition (CVPR) 2009*, pages 248–255.

Du, C., Du, C., and He, H. (2017). Sharing deep generative representation for perceived image reconstruction from human brain activity. In *International Joint Conference on Neural Networks (IJCNN) 2017*, pages 1049–1056.

Goodfellow, I., Pouget-Abadie, J., Mirza, M., Xu, B., Warde-Farley, D., Ozair, S., Courville, A., and Bengio, Y. (2014). Generative adversarial nets. In *Advances in Neural Information Processing Systems (NIPS) 2014*, pages 2672–2680.

Güçlütürk, Y., Güçlü, U., Seeliger, K., Bosch, S., van Lier, R., and van Gerven, M. A. (2017). Reconstructing perceived faces from brain activations with deep adversarial neural decoding. In *Advances in Neural Information Processing Systems (NIPS) 2017*, pages 4249–4260.

Güçlü, U. and van Gerven, M. (2013). Unsupervised learning of features for bayesian decoding in functional magnetic resonance imaging. In *22nd annual Belgian-Dutch Conference on Machine Learning (BeNeLearn) 2013*.

Hanke, M., Halchenko, Y. O., Sederberg, P. B., Hanson, S. J., Haxby, J. V., and Pollmann, S. (2009). PyMVPA: A python toolbox for multivariate pattern analysis of fMRI data. *Neuroinformatics*, 7(1):37–53.

Haxby, J. V. (2001). Distributed and overlapping representations of faces and objects in ventral temporal cortex. *Science*, 293(5539):2425–2430.

Haxby, J. V., Guntupalli, J. S., Connolly, A. C., Halchenko, Y. O., Conroy, B. R., Gobbini, M. I., Hanke, M., and Ramadge, P. J. (2011). A common, high-dimensional model of the representational space in human ventral temporal cortex. *Neuron*, 72(2):404–416.

Haynes, J.-D. (2015). A primer on pattern-based approaches to fMRI: Principles, pitfalls, and perspectives. *Neuron*, 87(2):257–270.

Horikawa, T. and Kamitani, Y. (2017). Generic decoding of seen and imagined objects using hierarchical visual features. *Nature Communications*, 8.

Huth, A. G., Lee, T., Nishimoto, S., Bilenko, N. Y., Vu, A. T., and Gallant, J. L. (2016). Decoding the semantic content of natural movies from human brain activity. *Frontiers in Systems Neuroscience*, 10(81).

Johnson, J., Alahi, A., and Fei-Fei, L. (2016). Perceptual losses for real-time style transfer and super-resolution. In *European Conference on Computer Vision (ECCV) 2016*, pages 694–711.

Kamitani, Y. and Tong, F. (2005). Decoding the visual and subjective contents of the human brain. *Nature Neuroscience*, 8(5):679–685.

Kay, K. N., Naselaris, T., Prenger, R. J., and Gallant, J. L. (2008). Identifying natural images from human brain activity. *Nature*, 452(7185):352–355.

Kingma, D. P. and Ba, J. (2014). Adam: A method for stochastic optimization. *arXiv preprint arXiv:1412.6980*.

Krizhevsky, A., Sutskever, I., and Hinton, G. E. (2012). ImageNet classification with deep convolutional neural networks. In *Advances in Neural Information Processing Systems (NIPS) 2012*, pages 1097–1105.

Lin, T.-Y., Maire, M., Belongie, S., Hays, J., Perona, P., Ramanan, D., Dollár, P., and Zitnick, C. L. (2014). Microsoft COCO: Common Objects in Context. In *European Conference on Computer Vision (ECCV) 2014*, pages 740–755.

Mason, W. and Suri, S. (2012). Conducting behavioral research on Amazon's Mechanical Turk. *Behavior Research Methods*, 44(1):1–23.

Miyawaki, Y., Uchida, H., Yamashita, O., Sato, M., Morito, Y., Tanabe, H. C., Sadato, N., and Kamitani, Y. (2008). Visual image reconstruction from human brain activity using a combination of multiscale local image decoders. *Neuron*, 60(5):915–929.

musyoku (2017). Code for the paper: Improved techniques for training GANs. github.com/musyoku/improved-gan. Commit: ba1e09f (--short).

Naselaris, T., Prenger, R. J., Kay, K. N., Oliver, M., and Gallant, J. L. (2009). Bayesian reconstruction of natural images from human brain activity. *Neuron*, 63(6):902–915.

Nishimoto, S., Vu, A. T., Naselaris, T., Benjamini, Y., Yu, B., and Gallant, J. L. (2011). Reconstructing visual experiences from brain activity evoked by natural movies. *Current Biology*, 21(19):1641–1646.

Parthasarathy, N., Batty, E., Falcon, W., Rutten, T., Rajpal, M., Chichilnisky, E., and Paninski, L. (2017). Neural networks for efficient bayesian decoding of natural images from retinal neurons. In *Advances in Neural Information Processing Systems (NIPS) 2017*, pages 6437–6448.

Radford, A., Metz, L., and Chintala, S. (2015). Unsupervised representation learning with deep convolutional generative adversarial networks. *arXiv preprint arXiv:1511.06434*.

Ridgeway, K., Snell, J., Roads, B., Zemel, R. S., and Mozer, M. C. (2015). Learning to generate images with perceptual similarity metrics. *arXiv preprint arxiv:1511.06409*.

Salimans, T., Goodfellow, I., Zaremba, W., Cheung, V., Radford, A., and Chen, X. (2016). Improved techniques for training GANs. In *Advances in Neural Information Processing Systems (NIPS) 2016*, pages 2234–2242.

Salzberg, S. L. (1997). On comparing classifiers: Pitfalls to avoid and a recommended approach. *Data Mining and Knowledge Discovery*, 328:317–328.

Schoenmakers, S., Barth, M., Heskes, T., and van Gerven, M. A. J. (2013). Linear reconstruction of perceived images from human brain activity. *NeuroImage*, 83:951–961.

Schoenmakers, S., Güçlü, U., van Gerven, M. A. J., and Heskes, T. (2015). Gaussian mixture models and semantic gating improve reconstructions from human brain activity. *Frontiers in Computational Neuroscience*, 8:173.

Schomaker, L. and Vuurpijl, L. (2000). Forensic writer identification: A benchmark data set and a comparison of two systems [internal report for the Netherlands Forensic Institute].

Stanley, G. B., Li, F. F., and Dan, Y. (1999). Reconstruction of natural scenes from ensemble responses in the lateral geniculate nucleus. *Journal of Neuroscience*, 19(18):8036–8042.

Thirion, B., Duchesnay, E., Hubbard, E., Dubois, J., Poline, J. B., Lebihan, D., and Dehaene, S. (2006). Inverse retinotopy: Inferring the visual content of images from brain activation patterns. *NeuroImage*, 33(4):1104–1116.

Tokui, S., Oono, K., Hido, S., and Clayton, J. (2015). Chainer: A next-generation open source framework for deep learning. In *Workshop on Machine Learning Systems (LearningSys) during Advances in Neural Information Processing Systems (NIPS) 2015*.

Van der Maaten, L. (2009). A new benchmark dataset for handwritten character recognition. *Tilburg University*.